JOURNAL OF PROPULSION AND POWER
Vol. 16, No. 3, May–June 2000

Incidence Effects on Wake-Induced Transition on an Axial Compressor Blade

W. J. Solomon*
Ohio Aerospace Institute/General Electric Aircraft Engines, Cincinnati, Ohio 45215
and
G. J. Walker†
University of Tasmania, Hobart, Tasmania 7001, Australia

Boundary-layer transition phenomena on an outlet stator blade of a 1.5-stage axial compressor were observed with a closely packed array of hot-film sensors. Synchronized sampling was used to identify periodic features associated with the passage of rotor wakes; ensemble-averaged wall shear stress, unsteadiness, and intermittency are presented. Three flow cases at different blade incidence are examined to determine the effects of surface pressure distribution on the transition behavior. Wake-induced transitional strips occur in all cases; their nature and the relative strength of associated calming periods and periodic unsteadiness are strongly influenced by the blade incidence. A significant difference in character between wake-induced transition effects on the suction and pressure surfaces is observed. Periodic phenomena are still evident when transition is initiated within a midchord separation bubble.

Nomenclature

c	= blade chord
E	= hot-film anemometer output voltage
E_0	= anemometer voltage at zero flow
i	= blade incidence
k	= film calibration constant
Q	= total heat transfer from film gauge
Q_s	= heat transfer from film gauge to the substrate
Q_0	= heat transfer from film gauge at zero flow
Re_{mb}	= rotor blade Reynolds number, $U_{\mathrm{mb}}c/\nu$
Re_1	= stator blade inlet Reynolds number, $U_1 c/\nu$
S	= maximum surface distance
s	= surface distance
s^*	= nondimensional surface distance from leading edge, s/S
T	= rotor blade passing period
t	= time
t^*	= nondimensional time, t/T
U	= local freestream velocity
U_{mb}	= rotor blade velocity at midblade height
U_1	= blade row inlet relative velocity
V_a	= inlet axial velocity
γ	= turbulent intermittency
ΔT_0	= temperature elevation of hot-film gauge
Δt	= data acquisition sampling period
ν	= kinematic viscosity
τ	= quasi-wall shear stress [Eq. (1)]
$\bar{\tau}$	= long-term mean quasi-wall shear stress
τ_w	= wall shear stress
$\langle\tau(i)\rangle$	= ensemble average τ at time t equal to $t_0 + i\Delta t$
$\langle\tau(i)\rangle_{\mathrm{rms}}$	= ensemble random unsteadiness of τ
ϕ	= flow coefficient, V_a/U_{mb}

Introduction

THE study of wake-induced transition and the influence of freestream turbulence on the flow around turbine blades has received a great deal of attention due to the importance of transitional flow and heat transfer in the turbine environment. Early investigators such as Turner[1] and Hodson[2] used time-mean measurements of surface heat transfer distributions to examine the influence of freestream disturbances on the boundary-layer behavior. Later workers[2–10] used time-resolved measurements from small-surface film gauges to monitor individual turbulent breakdown events and track the development of wake-induced transition on turbine airfoils. The review by Mayle[11] contains a comprehensive bibliography of this research.

The problem of unsteady transition on axial compressor blades has received comparatively little attention, with many workers believing that the boundary layer on a compressor blade would be predominantly turbulent. However, the hot-wire studies of Walker[12–14] and Walker et al.[15] clearly established the existence of extensive laminar flow regions on an axial compressor stator and provided the first evidence of unsteady transition phenomena on axial compressor blades in response to passing rotor wakes. Hansen and Okiishi[16] used surface hot-film gauges mounted at intervals of 25% chord to study wake-induced transition on an axial compressor stator. Detailed hot-wire investigations of transitional flow phenomena in a compressor cascade both with and without incident wakes have been reported by Dong and Cumpsty.[17,18]

Halstead et al.[19] have recently made comprehensive surveys of boundary-layer transition behavior in multi-stage axial compressors and turbines using closely spaced arrays of hot-film gauges and hot-wire instrumentation. This work has revealed remarkable similarities in flow behavior between the two types of machine and clearly establishes the importance of wake-induced transition phenomena in delaying separation on axial compressor blades. A comparison of these results with the parallel study by Solomon and Walker[20] in a 1.5-stage axial compressor indicates that the essential features of transition in an embedded stage of a multistage machine are modeled when there is one full stage upstream of the blade row under test.

The present investigation extends the work of Solomon and Walker[20] to examine the effects of incidence changes on wake-induced transition behavior on the outlet stator of the test compressor. Measurements from an array of 61 hot-film gauges around the blade circumference are presented. The surface pressure distribution significantly influences the transition phenomena, both as regards the effects of changing incidence and the differences in transition behavior between the suction and pressure surfaces of the blade. In the conclusion, the resulting implications for compressor blade design are discussed.

Received 10 May 1996; revision received 17 March 1999; accepted for publication 2 June 1999.

*Senior Research Associate, MS A411, One Neumann Way.
†Reader in Mechanical Engineering, GPO Box 252-65, School of Engineering.

Equipment and Test Cases

Research Compressor

The research compressor is a 1.5-stage axial flow machine with a 37-blade rotor, a 38-blade inlet guide vane (IGV) row, and a 38-blade stator row. The blades have a nominal chord of 76.2 mm and are machined to C4 profiles on circular arc camber lines. The hub diameter is 686 mm, the tip diameter 1143 mm, and the blade aspect ratio is 3.0. At midblade height the pitch/chord ratio is 1.02 for the rotor and 0.99 for the stationary rows. The IGV has an inlet blade angle of 0 deg (from axial) and an outlet blade angle of 27.8 deg at midblade height. The corresponding blade angles for the rotor and stator rows are 45 deg at the inlet and 14 deg at the outlet. The axial clearances for these tests were 1.17c between the IGV trailing edge and the rotor leading edge and 1.05c between the rotor and stator. Figure 1 shows a cross section of the compressor blading at midblade height. A full description of this machine may be found by Oliver.[21]

A cylindrical sliding throttle at the outlet of an annular diffuser downstream of the compressor is used to adjust the throughflow. The compressor is driven by a variable speed dc drive; an optical shaft encoder generating 6000 pulses/rev is used to obtain rotor speed and also provides a zero-marker signal for synchronized sampling.

The inlet axial velocity is found using a pitot-static probe mounted upstream of the IGV row. Inlet temperature is measured using a platinum resistance thermometer. Capacitative transducers are used to measure ambient pressure and inlet dynamic pressure. All low-speed data acquisition and control of the compressor speed and throttle position is performed by an IBM-compatible personal computer.

Test Cases

The three test cases presented here examine the influence of incidence on the stator blade surface transition behavior for a machine Reynolds number based on chord and rotor midblade velocity, $Re_{\mathrm{mb}} = 1.2 \times 10^5$. At standard atmospheric conditions this corresponds to a rotor speed of 481 rpm and a midblade velocity U_{mb} of 23.0 m/s. The actual speed changed through the tests according to ambient temperature and pressure. Note that for constant Reynolds number operation there is a slight variation in the Reynolds number based on stator blade inlet velocity, Re_1, as the incidence changes.

The flow coefficient and, hence, the incidence was set for each of the three cases by positioning the sliding throttle. A summary of the test conditions is given in Table 1.

Table 1 Summary of test cases incidence variation

Re_1	i, deg	ϕ
1.07×10^5	2.9	0.60
1.12×10^5	−0.3	0.68
1.23×10^5	−8.2	0.84

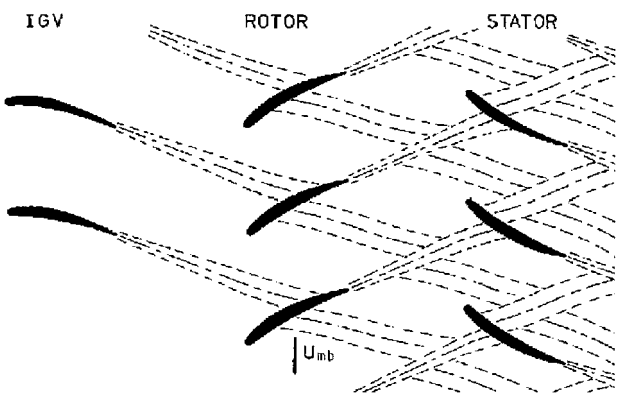

Fig. 1 Cross section of compressor blading, showing typical instantaneous wake dispersion.

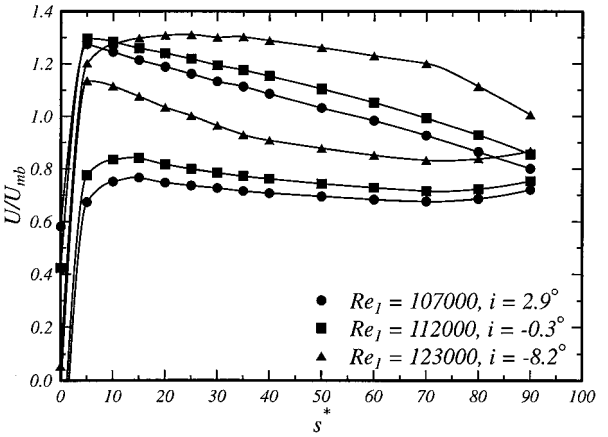

Fig. 2 Blade surface velocity distributions from pressure tappings.

The stator surface velocity distributions obtained from pressure tappings at midblade height are shown in Fig. 2. These velocity measurements were estimated to have an overall uncertainty of ±0.9% at 20:1 odds. At the two higher incidence values of 2.9 and −0.3 deg, the suction surface distribution is fairly linear and exhibits a moderate deceleration from a peak near 5% chord up to the trailing edge. On the pressure surface, there is a mild deceleration up to 70% chord from an initial peak near 15% chord followed by a slight acceleration over the rest of the surface. At the lower incidence value of −8.2 deg, the suction surface distribution has become convex with a peak around 30% chord and a discontinuity in slope around 70% chord indicating the presence of a laminar separation bubble. The pressure surface distribution is now markedly concave, with a strong deceleration immediately following the peak velocity around 5% chord.

As shown in Fig. 1, the stator is subjected to a disturbance field characterized by the regular passage of rotor wakes and the dispersed segments of IGV wakes produced by rotor blade chopping. The presence of a full stage upstream means that the unsteady flowfield seen by the stator is essentially similar to that experienced by an embedded stage of a multistage axial machine. Previous measurements indicate that the long-term average total disturbance level in the stator blade passage around midchord was about 3%.

Hot-Film Measurements and Data Processing

Hot-Film Anemometry Technique

One stator blade was instrumented with an array of 61 hot-film gauges spaced at intervals of 2.54 mm around the whole circumference at midblade height. Groups of up to five gauges were operated simultaneously using TSI model 150 anemometer bridges. A spacing of one inactive gauge between each operating gauge was allowed to minimize cross talk from substrate conduction. The frequency response of the hot films was estimated to be ≃ 30 kHz using the square wave test of Freymuth and Fingerson.[22] There were minor variations between different sensor/anemometer combinations.

Each anemometer output was sampled simultaneously at 50 kHz per channel and was ac coupled with a high-pass filter setting of 0.1 Hz. A low-pass filter at 20 kHz was used to eliminate aliasing. Power spectral density calculations indicated that most of the signal energy lay below 10 kHz except for a narrow band of anemometer power supply noise at around 15 kHz. A gain of ×50 or ×100 was chosen to give the maximum signal-to-noise ratio without saturating the input of the 12-bit A/D converter card. The dc levels at zero flow and at the operating point were recorded manually from the TSI digital voltmeter display.

Accurate calibration of individual sensors was not possible with the sensor array glued to the blade surface. Instead a semiquantitative method developed by Hodson et al.[9] was used to reduce the data. Liepmann and Skinner[23] have shown that the total power dissipation $Q = I^2 R_S$ for a hot film in a boundary layer is related to the wall shear stress τ_w by the expression $\tau_w^{1/3} \propto I^2 R_S / \Delta T_0$, provided

the thermal layer of the sensor lies within the linear region of the velocity distribution. The total heat loss from the sensor includes conduction from the sensor to the substrate, which is assumed to be independent of τ_w. As a first approximation (neglecting free convection at zero flow) this conductive term is equal to the total heat loss from the sensor at zero flow, Q_0. Thus, $(Q - Q_0)/\Delta T_0 = k\tau_w^{1/3}$ where k is the calibration constant of the film. Because $Q \propto E^2$ (anemometer voltage squared) and assuming $\Delta T_0 \propto E_0^2$, we have

$$\tau_w \propto \left(\frac{E^2 - E_0^2}{E_0^2}\right)^3 = \tau \tag{1}$$

Normalization with E_0^2 has the added advantage of reducing effects of variation in sensor size, resistance, etc. The term on the right-hand side (RHS) of Eq. (1) is plotted. This will be referred to as quasi-shear stress τ and is nondimensional. This term is effectively τ_w normalized by the film calibration coefficient.

Experimental Uncertainty in Quasi-Shear Stress

The experimental uncertainty associated with measurement of quasi-shear stress has been estimated by differentiating Eq. (1) with respect to E and E_0 and combining the errors as a sum of squares. The resulting expression for uncertainty in quasi-shear stress is

$$\frac{\partial\tau}{\tau} = 6\frac{E^2}{E^2 - E_0^2}\sqrt{\left(\frac{\partial E}{E}\right)^2 + \left(\frac{\partial E_0}{E_0}\right)^2} \tag{2}$$

For the sensor operating conditions used, $E^2/(E^2 - E_0^2)$ was approximately 13. Mean values of E and E_0 were determined from the TSI anemometer to an accuracy of $\pm 0.09\%$. Consequently, the mean value of quasi-shear stress τ was measured to an accuracy of approximately $\pm 10\%$. This is the uncertainty associated with measuring the quasi-shear stress and is not related to the difference between quasi-shear stress and the true wall shear stress. Estimation of the calibration constant required to convert τ to τ_w was not attempted in the current work.

Ensemble Statistics

Sampling of data was triggered by a rotor zero marker signal from the machine shaft encoder. For each case, the sampling period chosen was longer than five times the rotor blade passing period. By the use of this repeated sampling technique, periodic features of the flow can be resolved. Typically, $k = 1, \ldots, 512$ ensembles, each with $i = 1, \ldots, 1024$ instantaneous samples, $\tau(i, k)$ were taken. The ensemble average of quasi-shear stress $\langle\tau(i)\rangle$ is defined as

$$\langle\tau(i)\rangle = \frac{1}{n}\sum_{k=1}^{n}\tau(i, k) \tag{3}$$

The ensemble variance of τ is obtained from

$$\langle\tau(i)\rangle_{\text{rms}} = \left[\frac{1}{n}\sum_{k=1}^{n}(\tau(i, k) - \langle\tau(i)\rangle)^2\right]^{\frac{1}{2}} \tag{4}$$

Normalized ensemble rms values of τ were found from

$$\frac{\langle\tau(i)\rangle_{\text{rms}}}{\bar{\tau}} \tag{5}$$

Intermittency

The determination of turbulent intermittency from the hot-film gauge signals was based on a combination of the probability distribution function (PDF) method of Hazarika and Hirsch[24] and the peak–valley counting technique of Zohar[25] (see also Ref. 26). The first derivative of quasi-shear stress with respect to time was used as the detector.

The procedure commences by setting an initial value of the threshold for turbulence detection at about 0.7 times the standard deviation of the detector function. Regions where the threshold is exceeded are examined for peaks and valleys characteristic of fine-scale turbulent mixing, and the regions between any peaks and valleys are assigned an intermittency of 1.0 if the peaks and valleys are closer together than the specified window period. This gives a first guess of the intermittency distribution and allows the PDFs of the detector in laminar and turbulent zones to be evaluated.

A new value of the threshold is obtained from the intersection of the laminar and turbulent PDFs. It is assumed in this process that both PDFs are of Gaussian form. The procedure is then repeated until the threshold value converges to an acceptable accuracy and the resulting intermittency is determined.

Observations and Discussion

Individual Gauge Records

Figures 3a–3c show sets of typical records from individual gauges over the whole blade surface for the three flow cases investigated. The results are presented in the form of quasi-shear stress and plotted against dimensionless time in the form of rotor blade passing periods. Quasi-shear stress values have been normalized by the local value of long-term mean quasi-shear stress.

The composite pictures combine subsets of simultaneous samples from 5 neighboring gauges, with grouping of sensors sampled simultaneously indicated by numbers in parentheses in the right sidebar. Numbers along the left sidebar indicate the gauge location s^*. Samples are shown for every second gauge only. A solid linestyle is used to mark sections of each record identified as turbulent by the intermittency algorithm.

Results for the intermediate incidence case of $i = 0.3$ deg and Reynolds number $Re_1 = 1.12 \times 10^5$ are shown in Fig. 3b. The upper part of Fig. 3b shows strong evidence of wake-induced transition on the suction surface ($s^* > 0$). The wake-induced turbulent spots become apparent around $s^* = 0.2$. They grow steadily with distance downstream and exhibit the classic calming period with exponential recovery in shear stress toward the undisturbed state within the laminar region immediately following each spot. The maximum amplitude is reached between $s^* = 0.5$ and 0.6; here the appearance of the wake-induced spots is surprisingly regular, their leading edges are very sharply defined, and there is little evidence of Tollmien–Schlichting wave activity in the nonturbulent zones. Around $s^* = 0.7$ additional disturbances have started to appear in the remaining laminar regions. By $s^* = 0.92$ the flow between the wake-induced spots has become essentially turbulent, although some isolated laminar patches can still occasionally be seen. As reported by Solomon and Walker,[20] increasing the Reynolds number to $Re_1 = 1.6 \times 10^5$ at this incidence produces essentially similar suction surface flow behavior, with even greater regularity in the appearance of wake-induced turbulent spots and a slight forward shift of the transitional flow region.

For the higher incidence case of $i = 2.9$ deg shown in Fig. 3a the onset of wake-induced transition on the suction surface has moved forward to around $s^* = 0.1$. The wake-induced turbulent spots have become weaker, and there is more evidence of other disturbances appearing in the relaxing nonturbulent flow regions between them. At the lower incidence of $i = -8.2$ deg, there is very little evidence of turbulent activity on the suction surface until $s^* = 0.73$, where reattachment of transitional flow from a laminar separation bubble commencing around $s^* = 0.60$ can be seen. Transition is completed very rapidly in this case, but interestingly, there is still strong evidence of regular wake-induced turbulent spots from the gauge at $s^* = 0.73$ despite transition having been initiated within the bubble.

In all three cases, large spikes typical of turbulent breakdown events are occasionally evident from the last gauge on the suction surface at $0.98s^*$. The large magnitude of these spikes could be an artifact of the low values of long-term mean quasi-shear stress used to normalize the records at this position (see Fig. 4).

The flow behavior on the pressure surface (lower-half of Fig. 3, $s^* < 0$) is quite different in all three cases. Wake-induced turbulent spots are again present, but they are much weaker and more irregular in their appearance. The associated calming and relaxation effects are similarly weak. There is now frequent evidence

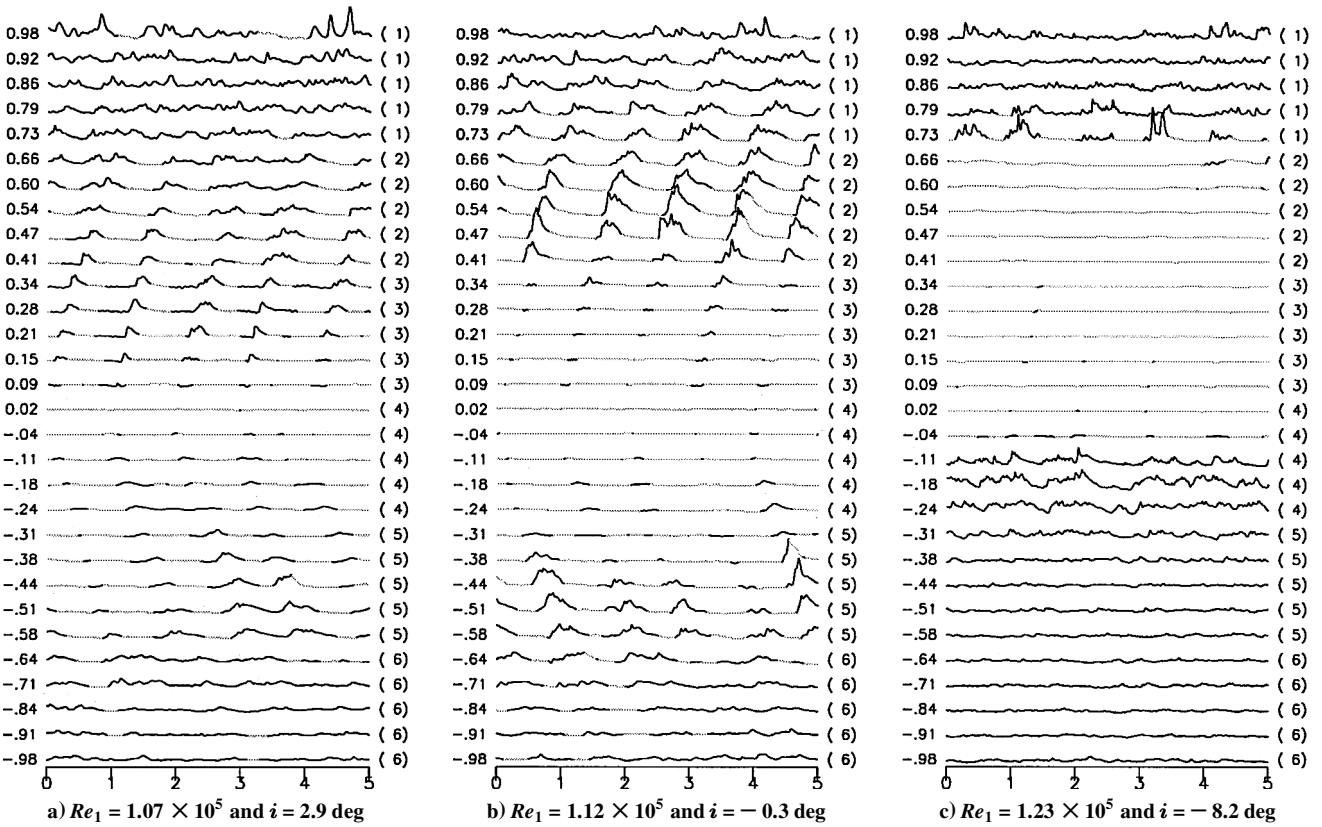

Fig. 3 Typical individual quasi-shear stress records over the whole blade surface: solid linestyle indicates regions identified as turbulent, $s^* = 0$ at stator leading edge, $s^* < 0$ corresponds to pressure surface.

of higher-frequency disturbances characteristic of Tollmien–Schlichting waves and examples of breakdown occurring from packets of such waves (for example, set 5 in Fig. 3b). The extent of transition on the pressure surface varies significantly with incidence: It is essentially completed by $s^* = 0.3$ at $i = -8.2$ deg, due to the leading-edge separation bubble induced by the strong adverse pressure gradient; the transition region steadily lengthens as incidence increases, and the pressure gradient near the leading edge becomes milder; at $i = 2.9$ deg practically the whole of the pressure surface flow is transitional.

Temporal Means and Envelopes of Quasi-Wall Shear Stress

Figure 4 shows the variation along the blade surface of various temporal mean values of gauge output, together with the envelopes of instantaneous maximum and minimum values. The results are plotted as quasi-shear stress τ. A logarithmic scale is used to accommodate the wide range of values of this variable. The central solid curve represents the long-term time-mean value for each gauge, $\bar{\tau}$. This gives an indication of the general boundary-layer development and the onset of transition and separation. The immediately adjacent long-dash curves represent the maximum and minimum ensemble average values over the whole sampling period. Their displacement indicates the magnitude of periodic unsteadiness in the flow. The outer short-dash curves correspond to the instantaneous maxima and minima of gauge readings over the whole sampling period. Their displacement is due to a combination of periodic and random unsteadiness but principally reflects the random component of gauge fluctuations.

Figures 4a–4c present results for the three different cases studied. All show a local minimum value of $\bar{\tau}$ in the stagnation region at the leading edge, followed by local maxima in the adjacent regions of strong acceleration up to about $s^* = 0.05$ on both suction and pressure surfaces. The separation of envelopes for ensemble mean and instantaneous values is masked in this region by the steep gradient of the curves. On the suction surface ($s^* > 0$) at $i = 2.9$ deg, there is a general tendency for $\bar{\tau}$ to fall as the pressure gradient becomes increasingly adverse toward the trailing edge. This is resisted by the progress of wake-induced transition around midchord, but even the resulting turbulent layer is unable to withstand the strong gradients for $s^* > 0.9$, where $\bar{\tau}$ falls rapidly and turbulent separation is approached. With reducing incidence, the rearward movement of the transition zone induced by the changing surface pressure distribution eventually results in the development of laminar separation on the suction surface; this is particularly evident at $i = -8.2$ deg, where local minima appear in all curves around $s^* = 0.7$.

On the pressure surface, the values of $\bar{\tau}$ generally fall in response to the positive pressure gradient near the leading edge, but subsequently increase in the region of accelerating flow over the rearward part of the blade. The sharp local minimum in $\bar{\tau}$ at $s^* = -0.08$ for $i = -8.2$ deg indicates the presence of a leading-edge separation bubble. The gauge nearest the trailing edge exhibits a sharp decrease in shear stress at all incidence values.

The displacement between the ensemble average envelope curves gives a useful indication of the degree of periodic unsteadiness and the progress of wake-induced transition. On the suction surface, the greatest separation of these curves occurs for the intermediate incidence case, $i = -0.3$ deg; this is in accordance with the nature of the individual shear stress traces shown in Fig. 3. The point at which these curves diverge changes monotonically with incidence, however, with divergence becoming noticeable at $s^* = 0.1$, 0.2, and 0.6 as i decreases from 2.9 to −0.3 to −8.2 deg, respectively. The ensemble average envelope curves converge again around $s^* = 0.9$ in all cases. This places a downstream limit on the extent of wake-influenced transition, bearing in mind that periodic unsteadiness may persist for some distance into the fully turbulent flow region. The periodicity of flow on the pressure surface is rather smaller in magnitude, as indicated by the individual gauge records. Its extent is quite short where transition occurs through the leading-edge separation bubble at $i = -8.2$ deg. For the higher incidence cases, the periodic flow covers a much longer region around midchord.

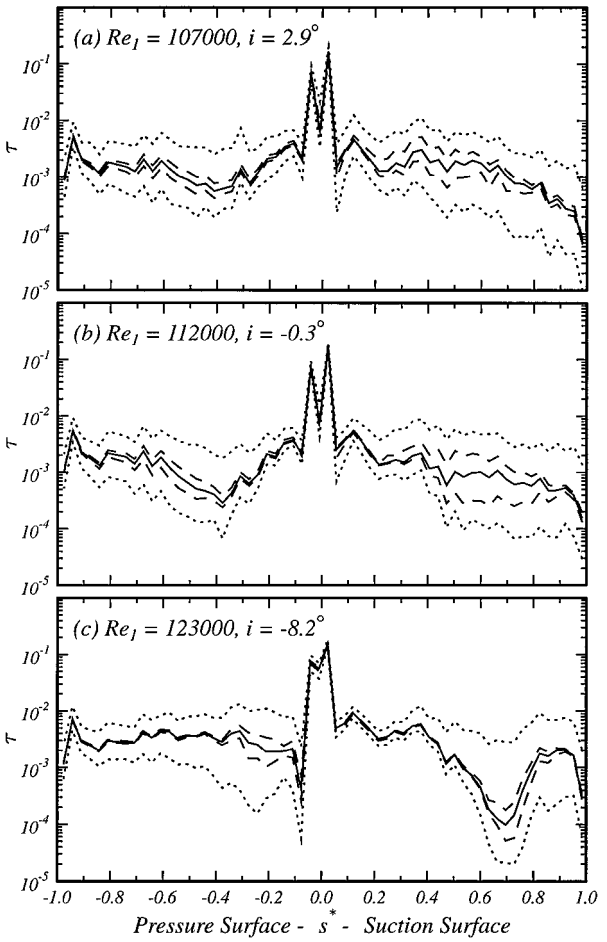

Fig. 4 Variation of long-term mean (——), maximum and minimum ensemble means (– – –), and maximum and minimum instantaneous values (----) of quasi-shear stress τ.

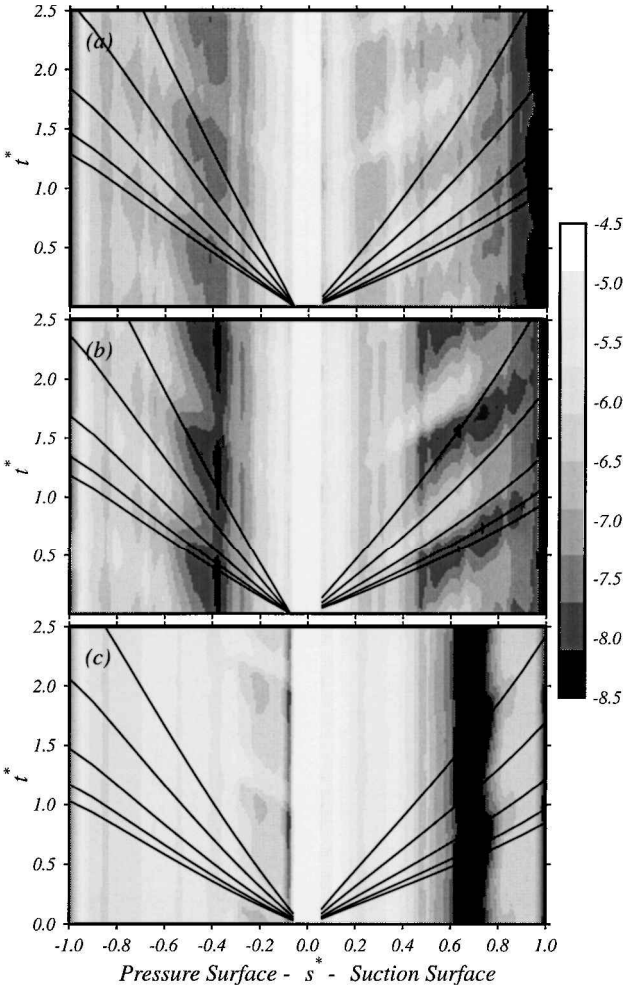

Fig. 5 Time–distance contour plot with particle trajectories for 1.0*U*, 0.88*U*, 0.7*U*, 0.5*U*, and 0.35*U* overlaid; log ensemble average quasi-shear stress: a) $i = 2.9$ deg, b) $i = -0.3$ deg, and c) $i = -8.2$ deg.

The divergence of the envelope curves for instantaneous values of τ is largely dependent on random shear stress fluctuations. This divergence commences quite close to the leading edge, where it probably reflects potential flow interactions associated with freestream turbulence. It subsequently increases to reach a maximum around the center of the transition zone and decreases to a lower value thereafter, although this is less evident on the suction surface where the flow is strongly decelerating. The ratio of divergence in the instantaneous τ envelopes to that of the ensemble average envelopes is noticeably greater where transition occurs through a separation bubble.

Time–Distance Contour Plots of Ensemble Average Data

Introduction

Time–distance contour plots of ensemble average quantities provide a convenient basis for presenting periodic unsteady flow data. Here normalized surface distance and time, s^* and t^*, have been used. To assist in the interpretation of periodic phenomena, these plots have been overlaid with the trajectories of particles traveling at 1.0, 0.88, 0.7, 0.5, and 0.35 times the freestream velocity; a lower slope corresponds to a higher convection velocity in this plot. These curves have been aligned so that the 1.0U trajectories coincide with the appearance of the wake center at $s^* = \pm 0.05$. The wake center was identified by finding the peak ensemble-averaged rms quasi-shear stress. The origin for t^* was taken as the time at which the wake center crossed the gauge closest to the leading edge and could be determined to a precision of ± 0.02.

The preceding set of convection velocities was chosen as follows. The trajectory at the local freestream velocity U indicates the path of the rotor wake over the stator blade surface. The values of 0.88U and 0.5U correspond to typical leading- and trailing-edge velocities of a turbulent spot in zero pressure gradient, as described by Schubauer and Klebanoff[27]; 0.7U is an approximate mean velocity of propagation for such a spot and for wake-induced turbulent strips.[28] The speed of 0.35U is a typical convection velocity for Tollmien–Schlichting waves; it also corresponds approximately to the trailing-edge velocity of the calmed region following a turbulent spot.[28]

Quasi-Shear Stress

Figure 5 shows time–distance contour plots of ensemble average quasi-shear stress $\langle \tau(i) \rangle$ for the three different incidence cases studied. Values are plotted on a log scale, as in Fig. 4, and the data for $-0.1 < s^* < 0.1$ is omitted to reduce the range of values covered. The semiregular vertical striations seen in Fig. 5 are a feature of all unnormalized plots of data from the surface film array. They arise partly from variations in the characteristics of individual gauges and partly from adjacent gauges being sampled at different times when the flow conditions may not have been exactly the same. Similar plots for simultaneously sampled data from alternate gauges only, presented by Solomon and Walker,[20] indicate a much lower degree of banding.

The general variation of $\bar{\tau}$ (corresponding to an average along $s^* = \text{const}$) with s^* is as described by Figs. 4a–4c. However, more detailed information about periodic phenomena is now available from the contour plots. In keeping with the individual gauge records shown in Figs. 3a–3c, the strongest periodicity is observed at the intermediate incidence case of $i = -0.3$ deg.

The suction surface plot for $i = -0.3$ deg shows a marked periodicity developing around $s^* = 0.3$. Farther downstream, there

are regular avenues of higher $\langle \tau(i) \rangle$ that indicate the presence of wake-induced transitional strips. Their propagation clearly lags the wake path in the freestream (1.0U trajectory). Within these avenues, $\langle \tau(i) \rangle$ increases to reach a maximum at about $s^* = 0.6$ as transition develops; it subsequently falls again in response to the increasing pressure gradient. The degree of periodicity decays for $s^* > 0.6$, but there is still some noticeable unsteadiness at the gauge closest to the trailing edge. The contour gradients in the vertical direction ($s^* = \text{const}$) show a sharp rise as a wake-induced strip arrives and a slower fall in the relaxing laminar flow region following its passage. This is a further signature of the calming effect.

The periodic unsteadiness on the pressure surface at $i = -0.3$ deg is much smaller in magnitude. There is again evidence of wake-induced transition with the origin of increased shear lagging the wake. However, the resulting avenues of increased $\langle \tau(i) \rangle$ are less distinct, and the passing wakes seem to play more of a modulating role. The periodicity decays rapidly downstream of $s^* = -0.8$ and has effectively disappeared by $s^* = -0.9$.

The darker areas in Fig. 5 indicate regions of lower wall shear stress that may be associated with periodic or steady separation. At $i = -8.2$ deg there appear to be regions of essentially steady laminar flow separation around $s^* = -0.1$ on the pressure surface and between $s^* = 0.6$ and 0.7 on the suction surface. For the two higher incidence cases there may be some intermittent laminar separation from the pressure surface around $s^* = -0.4$; this is most evident at $i = -0.3$ deg. The dark band near $s^* = 1.0$, which increases in width as the incidence becomes positive, suggests the development of turbulent separation from the trailing edge on the suction surface.

RMS Quasi-Shear Stress (Unnormalized)

Plots of rms output from surface film gauges are frequently used to to follow the progress of laminar–turbulent transition (for example, see work by Addison and Hodson,[6] Halstead et al.,[8] and Solomon and Walker[20]). The long-term average rms value typically rises from a low background level at transition onset to a maximum around the center of the transition zone; it then decays to a somewhat higher level in the turbulent flow region as transition is completed.

Plots of un-normalized $\langle \tau(i) \rangle_{\text{rms}}$ for the three different incidence cases are shown in Figs. 6a–6c. Data for $-0.1 < s^* < 0.1$ have been omitted because of the large range of values involved. Figures 6a–6c exhibit the broad features of the wake-induced transition that were evident from the plot of $\langle \tau(i) \rangle$ in Fig. 5 and have the same sort of vertical banding associated with gauge nonuniformities. In addition, regions of high $\langle \tau(i) \rangle_{\text{rms}}$ downstream of the two laminar separation bubbles can be seen in Fig. 6c.

As discussed by Solomon and Walker,[20] the use of unnormalized values may give undue prominence to disturbances associated with the wake passage near the leading edge; in some cases there is a danger of these being erroneously interpreted as indicating the start of wake-induced transition. Other problems with the unnormalized plots are 1) a loss of detail toward the trailing edge on the suction surface as both $\langle \tau(i) \rangle$ and $\langle \tau(i) \rangle_{\text{rms}}$ fall to low levels in the increasingly positive pressure gradient and 2) a peak of $\langle \tau(i) \rangle$ extending over a broad range of s^* on the suction surface that does not clearly indicate the center of the transition zone.

Normalized RMS Quasi-Shear Stress

Solomon and Walker[20] found that the aforementioned problems could be largely overcome by normalizing $\langle \tau(i) \rangle_{\text{rms}}$ with respect to the local long-term mean value, $\bar{\tau}$, as shown in Fig. 7. This method of data presentation significantly reduces the high values at the leading edge and amplifies the low values near the trailing edge, while substantially eliminating the banding associated with different gauge properties and alternate gauge sampling. The periodic features of the flow and the progress of transition are, thus, made more clearly evident; the peak normalized rms location is now more tightly defined and corresponds quite closely to the estimated center of the transition zone.

For the two higher incidence cases, the regions of high $\langle \tau(i) \rangle_{\text{rms}} / \bar{\tau}$ agree closely with the regions of high $\langle \tau(i) \rangle$. However, there is a tendency for the high normalized rms strip to precede the high

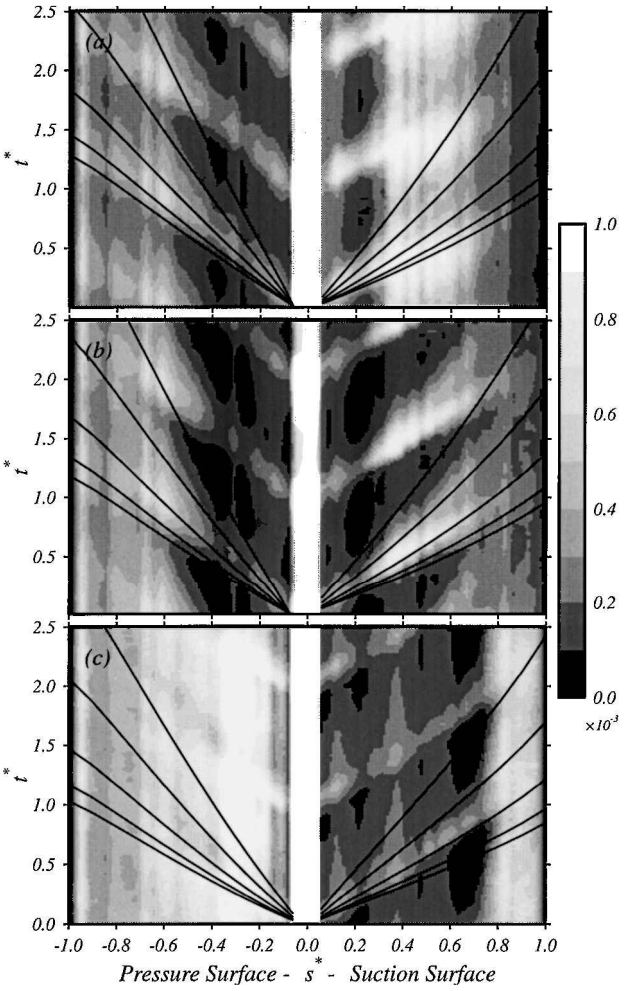

Fig. 6 Time–distance contour plot with particle trajectories for 1.0U, 0.88U, 0.7U, 0.5U, and 0.35U overlaid; ensemble average rms quasi-shear stress (unnormalized): a) i = 2.9 deg, b) i = −0.3 deg, and c) i = −8.2 deg.

shear strip, which is also evident in the unnormalized rms plot. This reflects unsteadiness in the arrival times of the rotor wakes and their associated transitional strips as the flow switches between laminar and turbulent in different realizations.

The normalization process introduces some distortions in regions of flow separation where the normalizing parameter $\bar{\tau}$ is very small. This produces very high values of $\langle \tau(i) \rangle_{\text{rms}} / \bar{\tau}$ in the regions of steady separation at $i = -8.2$ deg that were noted earlier. This feature can however assist in identifying regions of intermittent separation, as can be seen from the plot of normalized rms for $i = 2.9$ deg shown in Fig. 7a. Here there is a region of high $\langle \tau(i) \rangle_{\text{rms}} / \bar{\tau}$ immediately preceding the passage of the wake-induced transitional strip between $s^* = 0.4$ and 0.5 that suggests the occurrence of intermittent laminar separation; there is also some evidence of intermittent turbulent separation near the trailing edge on the suction surface.

Intermittency

Turbulent intermittency provides a convenient quantitative means of describing the progress of laminar–turbulent transition. It is also an essential parameter in several commonly used methods of calculating transitional boundary-layer development, such as eddy viscosity and linear combination integral techniques.

Gostelow et al.[29] showed that hot-wire measurements of peak intermittency (at about 20% of boundary-layer height) could be used to correlate data on the extent of transition obtained over a wide range of positive pressure gradients and freestream turbulence levels. The measured intermittency distributions all followed the universal similarity relationship of Narasimha[30] very closely, except for minor

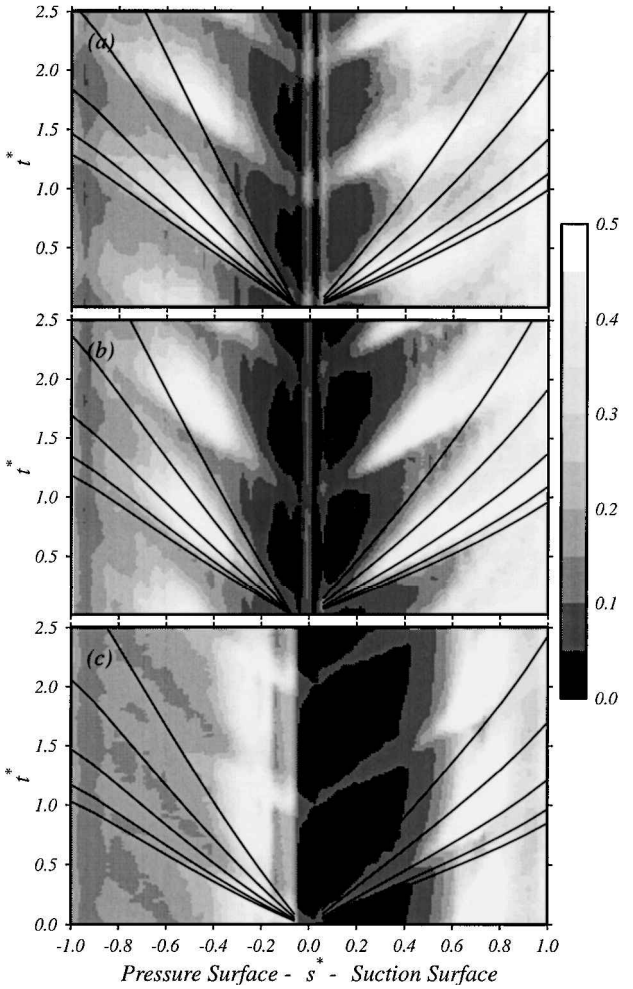

Fig. 7 Time–distance contour plot with particle trajectories for 1.0*U*, 0.88*U*, 0.7*U*, 0.5*U*, and 0.35*U* overlaid; ensemble average rms quasi-shear stress (normalized by local $\bar{\tau}$): a) $i = 2.9$ deg, b) $i = -0.3$ deg, and c) $i = -8.2$ deg.

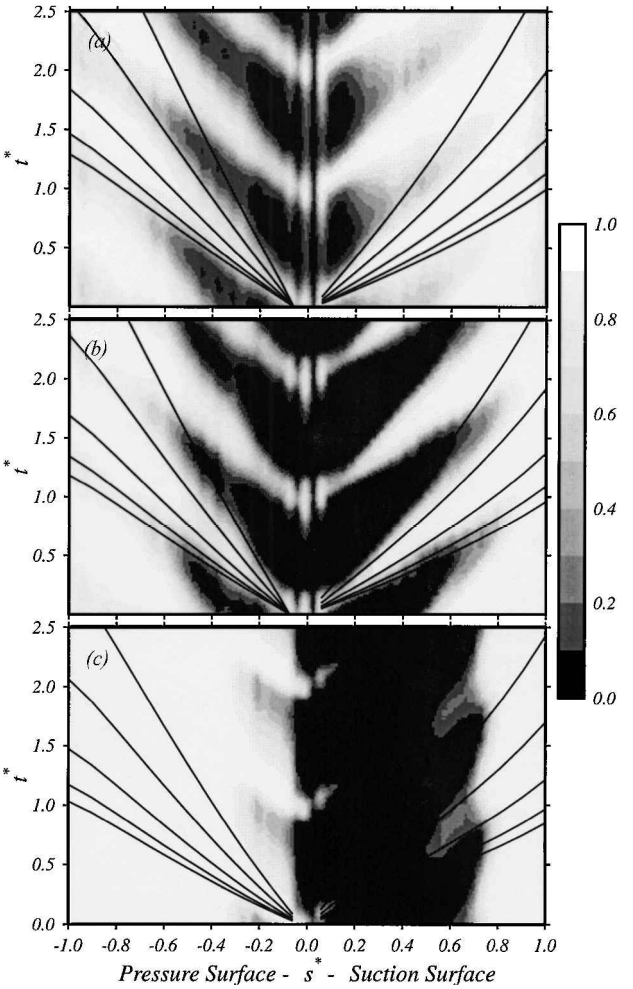

Fig. 8 Time–distance contour plot with particle trajectories for 1.0*U*, 0.88*U*, 0.7*U*, 0.5*U*, and 0.35*U* overlaid; ensemble average intermittency: a) $i = 2.9$ deg, b) $i = -0.3$ deg, and c) $i = -8.2$ deg.

deviations near the start of the transition zone; extrapolation of the fitted universal relationship from the central region of the transition zone provided a reliable quantitative basis for defining the start and end of transition.

Measurements of intermittency from surface hot-film gauges are necessarily more limited in usefulness. Quite good agreement between surface film and boundary-layer measurements can be expected where transition occurs in regions of constant pressure or accelerating flow. In decelerating flow, however, there is a well-known tendency for intermittency to fall toward the wall,[15,24] and this will result in surface film observations underestimating the true progress of transition within the most turbulent part of the wall layer. Where transition commences within the free shear layer over a laminar separation bubble, the onset of turbulence will not be visible to surface gauges until reattachment has commenced.

Contour plots of ensemble average intermittency from the surface film gauge array on the stator blade are presented in Fig. 8. These give a clearer indication of the progress and nature of transition than the previous methods of data presentation. At $i = 2.9$ deg, there is evidence of wake-induced transitional strips originating periodically from very close to the leading edge on the suction surface. Between these strips another mode of transition can be seen, and its completion is delayed until about $s^* = 0.8$ by the calming effect of the wake-induced strips. The drop in indicated intermittency close to the trailing edge probably results from turbulent separation; it is physically unrealistic to expect a drop in intermittency within the shear layer after transition has been completed in a positive pressure gradient. The marked vertical banding near the leading edge (which is also present in the normalized rms quasi-shear stress plots) is thought to result from spurious turbulent detections caused by marked fluctuations in τ arising from potential flow interactions associated with rotor wake chopping and freestream turbulence. On the pressure surface at $i = 2.9$ deg, the wake-induced transitional strips are much weaker; there is again evidence of transition occurring via other modes (natural or bypass) between these strips, where the flow remains transitional at the trailing edge.

At $i = -0.3$ deg, extensive wake-induced transitional strips are again present on the suction surface. The true origin of these strips is probably around $s^* = 0.2$, where a slight discontinuity in slope of their trajectories can be seen; downstream of this point the strips start to expand, and their mean convection rate falls to a value of about $0.6U$ characteristic of a growing turbulent spot in an adverse pressure gradient. The apparent transitional strips for $s^* < 0.2$ probably result from disturbances impressed on the boundary layer by the passing rotor wakes. The wake-induced strips on the suction surface are most highly developed in this particular case; their associated calming regions are accordingly much stronger and cause a significant delay in the completion of transition by other modes between the wake-induced strips. This results in the suction surface flow being transitional from about $s^* = 0.2$–0.9. Transition on the pressure surface closely resembles that at $i = 2.9$ deg, although there is a slightly later onset. This, and the reduced banding at the leading edge, could reflect lower levels of freestream turbulence and wake defect associated with reduced rotor loading.

At $i = -8.2$ deg, the intermittency distributions are markedly different. Apart from slight leading-edge interaction effects, there is no evidence of suction surface transition until about $s^* = 0.6$, where

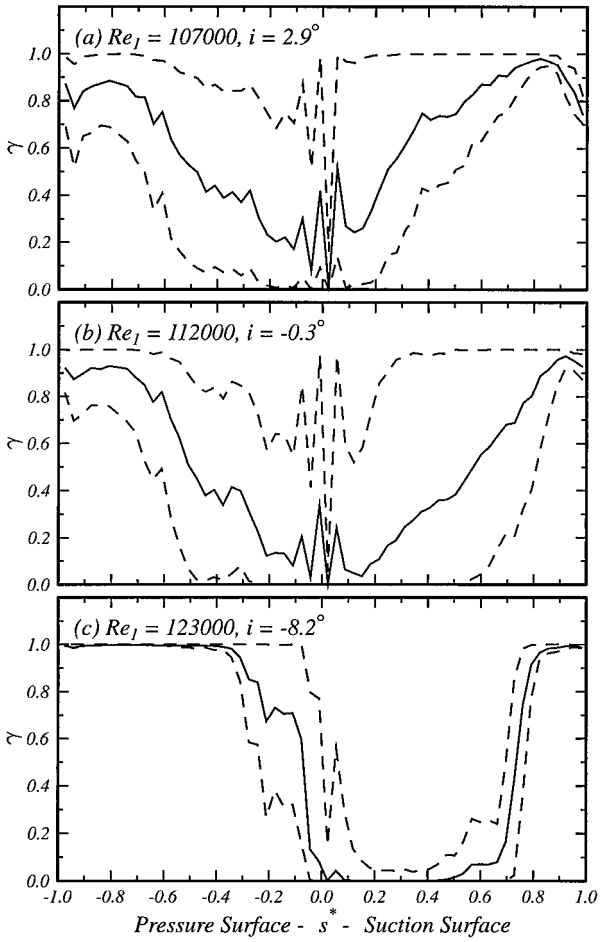

Fig. 9 Variation of long-term mean (——) and maximum and minimum ensemble means (– – –) of intermittency.

turbulent reattachment is commencing downstream of a laminar separation bubble. Interestingly, there is still evidence of wake-induced transition despite the turbulence having originated within a separated shear layer; however, the effect is rather weak, and there is little associated calming effect. On the pressure surface, transition is not completed until around $s^* = -0.3$ despite the apparent presence of some separation around $s^* = -0.1$. Transition occurs mainly through natural or bypass modes, except for narrow wake-induced strips that originate at the leading edge and are probably associated with leading-edge interactions.

The interpretation of the intermittency contour plots is assisted by presenting the plots of maximum and minimum ensemble average intermittency against chordwise position, which are shown in Fig. 9 together with the variation of long-term mean intermittency. It is necessary to ignore the fluctuations in these plots for $-0.1 < s^* < 0.1$ that are associated with the leading-edge interactions. The maximum ensemble mean indicates the progress of transition along the wake-induced path, whereas the minimum indicates the development of turbulent flow within the most calmed region between the wake-induced transitional strips; the separation of these two curves provides a further indication of periodic unsteadiness. The long-term mean intermittency provides a basis for comparing the experimental observations with the results of steady flow calculations.

A notable feature on the suction surface at $i = 2.9$ deg is the maximum ensemble average intermittency reaching 1.0 almost immediately at $s^* = 0$; this suggests the presence of a short leading-edge separation bubble as the rotor wake is cut by the stator leading edge. Other interesting features are the perturbations in all three curves observed on the pressure surface around $s^* = -0.2$, -0.24, and -0.4 for $i = -8.2$, -0.3, and 2.9 deg, respectively, which appear to be associated with intermittent laminar separation or turbulent reattachment phenomena. The fall in apparent intermittency associated with turbulent separation at the suction surface trailing edge, that appears at $i = -0.3$ deg and has expanded significantly at $i = 2.9$ deg is more clearly defined from these plots.

Conclusions

This paper has stressed the difficulties of interpreting flow data from surface hot-film arrays under arbitrary pressure gradient conditions. All of the data analysis techniques examined had certain individual problems and reflected the basic inability of surface gauges to provide useful information in regions of flow separation. An important aspect of this work has been the development of improved techniques for determining turbulent intermittency from surface film gauge measurements. This was found to give the most comprehensive and reliable picture of transitional flow behavior on an outlet stator of a 1.5-stage axial compressor.

The present observations are in full accordance with the more extensive survey of boundary layers in multi-stage compressors and turbines reported by Halstead et al.[19] They further emphasize the importance of periodic unsteadiness associated with wake-induced transition on axial turbomachine blades. The calming or relaxation region behind well-developed transitional strips has two important effects.

1) It greatly extends the length of transitional flow by delaying transition from other modes.

2) It delays the onset of laminar separation because of the periodic energizing of wall layer fluid by the wake-induced turbulent spots.

The present study has extended the work of Halstead et al.[19] by examining the transition behavior on blades with rather different forms of surface pressure distribution. The amplitude of periodic effects associated with wake-induced transition has been shown to vary greatly with incidence; this indicates in turn that there is potential for optimizing the design of turbomachine blade profiles through the choice of surface pressure distributions that will maximize the beneficial aspects of periodic transition phenomena. Further work is necessary to quantify the magnitude of wake-induced periodicity and its influence on separation and loss evolution so that these benefits can be achieved.

Acknowledgments

The authors gratefully acknowledge financial support from the Australian Research Council and Rolls–Royce, plc.

References

[1]Turner, A. B., "Local Heat Transfer Measurements on a Gas Turbine Blade," *Journal of Mechanical Engineering Science*, Vol. 13, No. 1, 1971, pp. 1–12.

[2]Hodson, H. P., "Boundary Layer Transition and Separation Near the Leading Edge of a High Speed Turbine Blade," *Journal of Engineering for Gas Turbines and Power*, Vol. 107, No. 1, April 1985, pp. 127–134.

[3]Sharma, O. P., Wells, R. A., Schlinker, R. H., and Bailey, D. A., "Boundary Layer Development on Turbine Airfoil Suction Surfaces," *Journal of Engineering for Power*, Vol. 104, No. 3, July 1982, pp. 698–706.

[4]Doorly, D. J., and Oldfield, M. L. G., "Simulation of Wake Passing in a Stationary Turbine Rotor Cascade," *Journal of Propulsion and Power*, Vol. 1, No. 4, 1985, pp. 316–318.

[5]LaGraff, J. E., Ashworth, D. A., and Schultz, D. L., "Measurement and Modelling of the Gas Turbine Blade Transition Process as Disturbed by Wakes," *Journal of Turbomachinery*, Vol. 111, No. 3, July 1989, pp. 315–322.

[6]Addison, J. S., and Hodson, H. P., "Unsteady Transition in an Axial Flow Turbine, Part 1: Measurements on the Turbine Rotor," *Journal of Turbomachinery*, Vol. 112, No. 2, 1990, pp. 206–214.

[7]Addison, J. S., and Hodson, H. P., "Unsteady Transition in an Axial Flow Turbine, Part 2: Cascade Measurements and Modeling," *Journal of Turbomachinery*, Vol. 112, No. 2, 1990, pp. 215–221.

[8]Halstead, D. E., Okiishi, T. H., and Wisler, D. C., "Boundary-Layer Transition and Separation on a Turbine Blade in Plane Cascade," AIAA Paper 90-2263, 1990.

[9]Hodson, H. P., Huntsman, I., and Steele, A. B., "An Investigation of Boundary Layer Development in a Multistage LP Turbine," *Journal of Turbomachinery*, Vol. 116, No. 3, July 1994, pp. 375-383.

[10]Schulte, V., and Hodson, H. P., "Wake-Separation Bubble Interaction in Low Pressure Turbines," AIAA Paper 94-2931, 1994.

[11]Mayle, R. E., "The Role of Laminar-Turbulent Transition in Gas Turbine

Engines," *Journal of Turbomachinery*, Vol. 113, No. 4, 1991, pp. 509–537.

[12]Walker, G. J., "The Prediction of Boundary Layer Development on Axial-Flow Turbomachine Blading," *Proceedings of 3rd Australasian Conference on Hydraulics and Fluid Mechanics*, Macmillan, New York, 1968.

[13]Walker, G. J., "The Unsteady Nature of Boundary Layer Transition on an Axial Compressor Blade," American Society of Mechanical Engineers, Paper 74-GT-135, 1974.

[14]Walker, G. J., "The Role of Laminar-Turbulent Transition in Gas Turbine Engines—A Discussion," *Journal of Turbomachinery*, Vol. 115, No. 2, 1993, pp. 207–217.

[15]Walker, G. J., Solomon, W. J., and Gostelow, J. P., "Observations of Wake-Induced Turbulent Spots on an Axial Compressor Blade," American Society of Mechanical Engineers, Paper 93-GT-378, 1993.

[16]Hansen, J. L., and Okiishi, T. H., "Rotor-Wake Influence on Axial-Compressor-Stator Boundary Layers," *Journal of Propulsion and Power*, Vol. 5, No. 1, 1989, pp. 89–94.

[17]Dong, Y., and Cumpsty, N. A., "Compressor Blade Boundary Layers: Part 1—Test Facility and Measurements with No Incident Wakes," *Journal of Turbomachinery*, Vol. 112, No. 2, 1990, pp. 222–230.

[18]Dong, Y., and Cumpsty, N. A., "Compressor Blade Boundary Layers: Part 2—Measurements with Incident Wakes," *Journal of Turbomachinery*, Vol. 112, No. 2, 1990, pp. 231–240.

[19]Halstead, D. E., Wisler, D. C., Okiishi, T. H., Walker, G. J., Hodson, H. P., and Shin, H., "Boundary Layer Development in Axial Compressors and Turbines: Part 1–4," American Society of Mechanical Engineers, Papers 95-GT-461–464, 1995.

[20]Solomon, W. J., and Walker, G. J., "Observations of Wake-Induced Transition on an Axial Compressor Blade," American Society of Mechanical Engineers, Paper 95-GT-381, 1995.

[21]Oliver, A. R., "Comparison Between Sand Cast and Machined Blades in the Vortex Wind Tunnel," Aeronautical Research Lab., Rept. ME 103, Melbourne, NSW, Australia, Sept. 1961.

[22]Freymuth, P., and Fingerson, L. M., "Electronic Testing of Frequency Response for Thermal Anemometers," *TSI Quarterly*, Vol. 3, Nov./Dec. 1977, pp. 5–12 (Appendix A of TSI IFA-100 manual).

[23]Liepmann, H., and Skinner, G., "Shearing Stress Measurements by Use of a Heated Element," NACA TN 3268, 1954.

[24]Hazarika, B. K., and Hirsch, C., "Transition over C4 Leading Edge and Measurement of Intermittency Factor Using PDF of Hot-Wire Signal," American Society of Mechanical Engineers, Paper 95-GT-294, 1995.

[25]Zohar, Y., "Fine Scale Mixing in a Free Shear Layer," Ph.D. Dissertation, Dept. of Mechanical and Aerospace Engineering, Univ. of California, Los Angeles, CA, April 1990.

[26]Zohar, Y., and Ho, C.-M., "Dissipation Scale and Control of Fine-Scale Turbulence in a Plane Mixing Layer," *Journal of Fluid Mechanics*, Vol. 320, 1996, pp 139–161.

[27]Schubauer, G. B., and Klebanoff, P. S., "Contributionson the Mechanics of Boundary Layer Transition," NACA TN 3489, Sept. 1955.

[28]Mayle, R. E., "Unsteady Multimode Transition in Gas Turbine Engines," AGARD Propulsion and Energetics Panel 80, 1992.

[29]Gostelow, J. P., Blunden, A. R., and Walker, G. J., "Effect of Free-Stream Turbulence and Adverse Presssure Gradients on Boundary Layer Transition," *Journal of Turbomachinery*, Vol. 116, No. 3, 1994, pp. 392–404.

[30]Narasimha, R., "The Laminar-Turbulent Transition Zone in the Boundary Layer," *Progress in Aerospace Science*, Vol. 22, No. 1, 1985, pp. 29–80.